CO2 discharge from the bottom of volcanic Lake Rotomahana, New Zealand

Mazot, Agnes; Schwandner, Florian M.; Christenson, Bruce; de Ronde, Cornel E. J.; Inguaggiato, Salvatore; Scott, Brad; Graham, Duncan; Britten, Karen; Keeman, J.; Tan, Karine

2014

Mazot, A., Schwandner, F. M., Christenson, B., de Ronde, C. E. J., Inguaggiato, S., Scott, B., et al. (2014). CO2 discharge from the bottom of volcanic Lake Rotomahana, New Zealand . Geochemistry, Geophysics, Geosystems, 15(3), 577-588.

https://hdl.handle.net/10356/104120

https://doi.org/10.1002/2013GC004945

Geochemistry Geophysics Geosystems G3

Article
Volume 15, Number 3
17 March 2014
doi: 10.1002/2013GC004945
ISSN: 1525-2027

Published by AGU and the Geochemical Society

CO_2 discharge from the bottom of volcanic Lake Rotomahana, New Zealand

Agnes Mazot
Department of Volcanology, GNS Science, Wairakei Research Centre, Private Bag 2000, Taupo 3352, New Zealand (a.mazot@gns.cri.nz)

Florian M. Schwandner
Earth Observatory of Singapore, Nanyang Technological University, Singapore, Singapore

Now at Jet Propulsion Laboratory, California Institute of Technology, Pasadena, California, USA

Bruce Christenson
National Isotope Centre, GNS Science, Lower Hutt, New Zealand

Cornel E. J. de Ronde
Department of Marine Geosciences, GNS Science, Lower Hutt, New Zealand

Salvatore Inguaggiato
Istituto Nazionale di Geofisica e Vulcanologia, Palermo, Italy

Brad Scott, Duncan Graham, and Karen Britten
Department of Volcanology, GNS Science, Wairakei Research Centre, Private Bag 2000, Taupo 3352, New Zealand

J. Keeman
Department of Geological Sciences, University of Canterbury, Christchurch, New Zealand

Karine Tan
Earth Observatory of Singapore, Nanyang Technological University, Singapore, Singapore

[1] From April 2010 to February 2011, CO_2 flux surveys were performed on Lake Rotomahana, New Zealand. The area has been hydrothermally active with fumaroles and sublacustrine hydrothermal activity before and since the eruption of Mt Tarawera in 1886. The total CO_2 emission from the lake calculated by sequential Gaussian simulation is 549 ± 72 t d^{-1}. Two different mechanisms of degassing, diffusion through the water-air interface and bubbling, are distinguished using a graphical statistical approach. The carbon dioxide budget calculated for the lake confirms that the main source of CO_2 to the atmosphere is by diffusion covering 94.5% of the lake area (mean CO_2 flux 25 g m^{-2} d^{-1}) and to a lesser extent, bubbling (mean CO_2 flux 1297 g m^{-2} d^{-1}). Mapping of the CO_2 flux over the entire lake, including over lake floor vents detected during the survey, correlates with eruption craters formed during the 1886 eruption. These surveys also follow regional tectonic patterns present in the southeastern sector of Lake Rotomahana suggesting a deep magmatic source (~10 km) for CO_2 and different pathways for the gas to escape to the surface. The values of $\delta^{13}C_{CO2}$ (−2.88 and −2.39‰) confirm the magmatic origin of CO_2.

Components: 7,694 words, 7 figures, 4 tables.

Keywords: Lake Rotomahana; CO_2 flux; bubbling and dissolved gases; carbon and helium isotopes; tectonics.

Index Terms: 8430 Volcanic gases: Volcanology; 8424 Hydrothermal systems: Volcanology; 8419 Volcano monitoring: Volcanology; 0450 Hydrothermal systems: Biogeosciences; 3017 Hydrothermal systems: Marine Geology and Geophysics; 3616 Hydrothermal systems: Mineralogy and Petrology; 4832 Hydrothermal systems: Oceanography: Biological and Chemical; 8135 Hydrothermal systems: Tectonophysics; 4302 Geological: Natural Hazards; 7280 Volcano seismology: Seismology; 1034 Hydrothermal systems: Geochemistry.

Received 17 July 2013; **Revised** 19 December 2013; **Accepted** 19 December 2013; **Published** 17 March 2014.

Mazot, A., F. M. Schwandner, B. Christenson, C. E. J. de Ronde, S. Inguaggiato, B. Scott, D. Graham, K. Britten, J. Keeman, and K. Tan (2014), CO_2 discharge from the bottom of volcanic Lake Rotomahana, New Zealand, *Geochem. Geophys. Geosyst.*, *15*, 577–588, doi:10.1002/2013GC004945.

1. Introduction

[2] Volcanic lakes are different from other natural lakes because of the input of magmatic gases derived from underlying magma chambers. These lakes are generally hotter and more concentrated [e.g., *Varekamp et al*., 2000]. Volcanic lakes may host various manifestations of hydrothermal activity on the lake floor, including hot springs, chimneys, pockmarks, and localized areas of mineralization [e.g., *de Ronde et al*., 2002]. The lake-atmosphere interface of volcanic lakes may exhibit a greater transfer of gases than lakes with no magmatic input, although this depends on the size of the crater and the number of sublacustrine vents discharging fluids on the lake floor [*Bernard et al*., 2004; *Bernard and Mazot*, 2004; *Mazot et al*., 2011]. In order to measure the gas flux from crater lakes it is necessary to measure their fluxes at the lake surface. Degassing through the lake surface is via bubbles, commonly seen as plumes ascending through the water column (i.e., convective/advective degassing), or by molecular diffusion through the water/air interface. Measurement of diffuse degassing from lakes using a floating accumulation chamber method has proved reliable for volcanic lakes worldwide [*Perez et al*., 2011].

[3] In this study, we report the first data on surface CO_2 flux (F_{CO2} values in g m^{-2} d^{-1}) from the volcanic Lake Rotomahana. A CO_2 budget for the lake is estimated to assist understanding the different possible contributions of CO_2 to the atmosphere. Results from chemical and isotopic compositions of bubbling and dissolved gases are presented and provide a better understanding of the Rotomahana/Waimangu hydrothermal system.

2. Geological and Volcanological Settings

[4] Lake Rotomahana is part of the Tarawera Volcanic Complex located in the southern part of the Okataina Volcanic Centre (OVC), the most recently active of the eight major rhyolite eruptive centers in the Taupo Volcanic Zone, North Island, New Zealand (Figure 1a) [*Nairn*, 2002]. Over the past ~26,000 years, rhyolitic and basaltic eruptions formed the Tarawera linear volcanic complex in the southern part of Haroharo caldera [*Nairn*, 2002]. Prior to the 1886 Tarawera eruption, the Rotomahana area was a site of numerous phreatic and magmatic eruptions and was host to an intensely active hydrothermal field with hot springs, geysers, fumaroles and two famous sinter terraces known as the Pink and White Terraces. Two small lakes occupied part of the site of present-day Lake Rotomahana: Lake Rotomahana (hot) and Lake Rotomakariri (cold) (Figure 1b). The most destructive manifestations of the 1886 Tarawera basaltic plinian fissure eruption occurred in the Rotomahana area. Phreatomagmatic and hydrothermal explosions ejected both hydrothermally altered and juvenile rocks, forming large explosion craters. Shortly after the eruption, the Rotomahana valley began filling with cold water. Today, hydrothermal activity in Lake Rotomahana is focused in the western part of the lake (Figure 1b) with numerous fumaroles, hot springs and geysers (known as Steaming Cliffs) occurring along the shoreline, and a number of bubbling areas clearly visible offshore.

[5] Eruptive activity occurred also to the southwest of Lake Rotomahana in the Waimangu area, with an explosive eruption recorded on August 1886 and a hydrothermal eruption in 1924 [*Nairn*, 2002]. Nowadays, the thermal activity consists of hot springs and crater lakes, fumaroles, hydrothermal eruption craters, steaming and altered ground, and minor silica deposits [*Mongillo*, 1994].

3. Sampling Procedures

[6] We used a West Systems flux instrument with a LICOR Li-800 nondispersive infrared CO_2

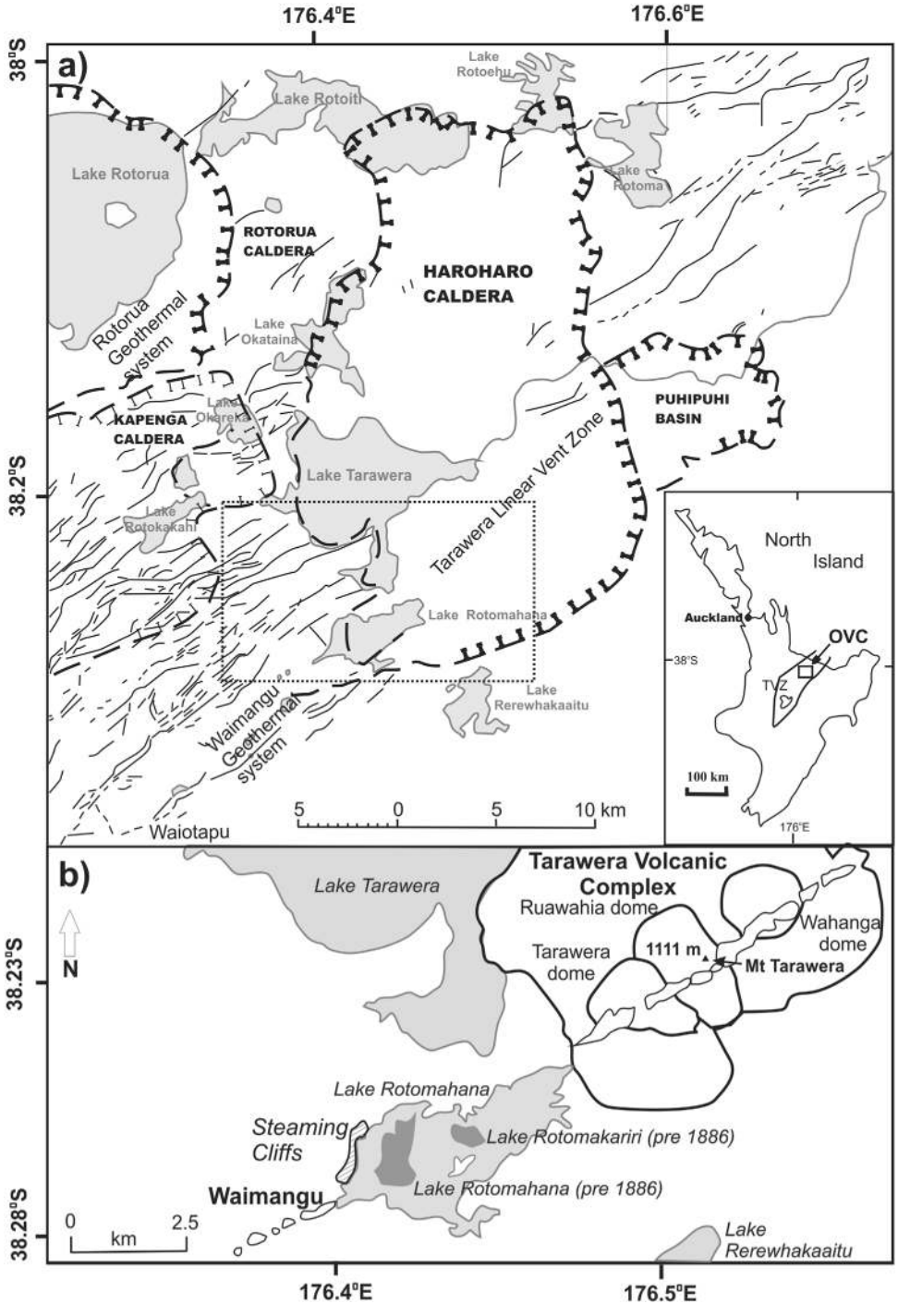

Figure 1. (a) Map of the Okataina Volcanic Centre (OVC) showing calderas and the faults (modified from *Shane et al*. [2008]). Inset: Map of the North Island of New Zealand showing the location of the Taupo Volcanic Zone. (b) Location map of Lake Rotomahana showing the location of the pre-1886 lakes Rotomahana and Rotomakariri in dark blue, superimposed on the modern lake area in light blue (modified from *Nairn* [2002]).

detector and the floating accumulation chamber method [*Mazot el al*., 2011] to measure CO_2 flux at the surface of Lake Rotomahana. The flux was measured over 10 field campaigns, from April 2010 to February 2011, and resulted in 484 points covering the entire lake area (Figure 2). Minimum and maximum wind speeds were measured 1 m above the surface of the lake as part of each flux measurement.

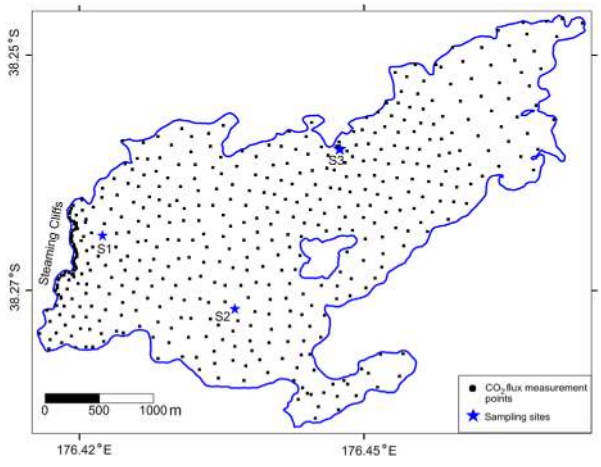

Figure 2. Point locations of the 484 CO_2 flux measurements made over 10 field campaigns from April 2010 to February 2011. Water sampled through the water column at S1 and S2, bubbling gases sampled at the surface of S1 and S3 and dissolved gases sampled at the surface of S3.

[7] Water samples were collected using Niskin-type sampler along vertical profiles between the lake floor and lake surface at two sites (S1 and S2) at maximum depths of 73 and 95 m, respectively (Figure 2). At both locations bubbles were seen to rise from the lake bottom to the surface. In conjunction with water sampling, vertical profiles of depth (±0.05 m), temperature (±0.01°C), Eh (±20 mV), and pH (±0.2) were measured with a Hydrolab MS5 multiparameter CTDx probe (Hach Environmental, Loveland, CO, USA) equipped with a data logger.

[8] Bubble gases were sampled at the surface using stopcock bottles (S1 and S3) and preevacuated Giggenbach flasks (S3). The depth of the lake at S3 was 1 m. Two samples of dissolved gases were collected at the surface of S3 using glass bottles that were hermetically sealed.

[9] On a separate survey (27 January 2011), we employed a FURUNO FCV echo sounder, recording data at 33, 200, and 582 kHz to image the gas streams (plumes) ascending from the lake floor. The echo sounder can record bubbles with a diameter as low as 0.6 mm. A FUGRO SeaSTAR satellite system provided navigation of the University of Waikato vessel M/V *Taitum*. This survey followed a previous magnetic survey that was oriented NNW-SSE direction with track spaced ~100 m. The vessel tracks were logged using Trimble HydroPro software. Only the bubble plumes encountered along these lines were recorded.

4. Analytical Procedures

[10] Cations, B, and SiO_2 were analyzed by inductively coupled plasma optical emission spectroscopy methods (ICP-OES). Anions were measured by ion chromatography (F, SO_4, NO_3, and Br) and titration (Cl and HCO_3).

[11] Bubble gases were sampled and analyzed for CO_2, O_2, N_2, Ar, CO, and CH_4 at GNS Science by methods described in *Christenson et al.* [2010b]. Dissolved gases from the sealed samples were analyzed according to the method described by *Capasso and Inguaggiato* [1998], which is based on the equilibrium partition of gas species between a liquid and a gas phase after the introduction of a host gas (Ar) into the sample. Dissolved gases were analyzed using a Perkin Elmer 8500 gas-chromatograph equipped with a 4 m long Carbosieve S II column and Ar as the carrier gas. He, H_2, O_2, N_2, and CO_2 were measured by means of a thermal conductivity detector (TCD), while CH_4 and CO were determined through a FID detector coupled with a methanizer. The $\delta^{13}C$ contents of total dissolved inorganic carbon (TDIC) of dissolved gases sampled at S3 were analyzed by a Finnigan Delta Plus mass spectrometer. Carbon isotopic values are expressed in δ versus the standard Pee Dee Belemnite (PDB), with an accuracy of 0.2‰. The determination of the helium isotopic composition was carried out at INGV, Palermo (Italy) on a static vacuum mass spectrometer (GVI Helix SFT) built for the simultaneous detection of ^3He and ^4He ion beam, to reduce the analytical error down to very low values (an average of ±0.05 Ra). The observed $^3He/^4He$ ratios are expressed relative to the atmospheric $^3He/^4He$ ratio (Ra) of 1.39×10^{-6}. The $^4He/^{20}Ne$ (further He/Ne) ratio was measured by a quadrupole mass spectrometer VG Masstor FX (accuracy ±5%). The measured $^3He/^4He$ are corrected for atmospheric contamination following *Sano et al.* [1987].

5. CO_2 Flux Data Processing

[12] Graphical statistical analysis (GSA) of the CO_2 flux data permits differentiation of populations of data that correspond to different ranges of flux values [*Chiodini et al.*, 1998, 2001; *Cardellini et al.*, 2003]. Different sources of degassing mechanism, in this case, degassing via bubble plume and by diffusion through the lake, can explain the different ranges of flux values. We partitioned the CO_2 flux data into different lognormal populations

Table 1. Chemical Composition (mg L^{-1}), Temperature (°C), pH, Total Dissolved Solids (TDS) of Lake Rotomahana Sampled at the Surface and Through the Water Column at S1 and S2 (see Figure 2)

Site	Depth (m)	Sampling Date	Temperature	pH	Na^+	K^+	Mg^{2+}	Ca^{2+}	Li^+	HCO_3^-	Cl^-	SO_4^{2-}	F^-	Br^-	NO_3^-	B	SiO_2	TDS
S1	0	22 Apr 2010	18.5	7.86	258	22.0	10.0	17.2	1.6	222	257	111	0.8	0.77	<0.03	2.2	114	903
	−35	25 Feb 2011	15.3	7.09	256	16.8	10.1	17.8	1.8	241	261	104	1.4	0.78	<0.03	2.6	122	920
	−68	1 Mar 2011	14.9	7.17	255	28.0	10.1	17.9	1.8	243	259	104	1.4	0.78	<0.03	2.5	122	919
	−73	24 Feb 2011	14.9	6.74	254	24.0	10.0	17.5	1.8	260	260	104	1.4	0.78	<0.01	2.5	120	936
S2	−45	3 Mar 2011	15.1	6.50	256	24.0	9.7	17.3	1.8	280	261	103	1.4	0.79	<0.03	2.3	112	957
	−95	3 Mar 2011	14.9	7.00	257	24.0	9.9	17.6	1.8	260	258	104	1.4	0.79	<0.03	2.3	115	937

where the proportion, the mean, and the standard deviation of each population are estimated following the procedure outlined by *Sinclair* [1974].

[13] The distribution of degassing areas across Lake Rotomahana, and estimates of the total CO_2 discharge from the lake, with associated errors, were derived by sequential Gaussian simulation (sGs) [*Deutsch and Journel*, 1998]. The measured CO_2 fluxes on the lake surface (Figure 2) were interpolated over a grid of square cells (50 × 50 m^2) covering the study area using the hole effect variogram model of *Deutsch and Journel* [1998]. The parameter values used for this model were 0.8, 1.05, and 2700 for nugget, sill, and range, respectively. This was followed by 500 sequential Gaussian simulations of the CO_2 fluxes. For each simulation, the CO_2 flux estimated at each cell is multiplied by 2500 m^2 (50 × 50 m cell size) and added to the other CO_2 fluxes estimated for neighborhood cells on the grid to obtain a total CO_2 output. The differences among all simulated maps were used to compute the uncertainty of the flux estimation [*Goovaerts*, 2001].

6. Results and Discussion

6.1. Chemical and Physical Characteristics of Lake Rotomahana

[14] The surface lake water has a pH of 7.86 with average water temperatures of 18.5°C in April 2010 and 23.6°C in February 2011 (Table 1). The chloride and sulfate concentrations are 257 and 111 ppm, respectively. Conductivity, temperature, and redox potential (Eh) at various depth form S1 and S2 are given in Table 1 and plotted in Figure 3. During sampling bubbles were visible on the surface at both of the sites. The lake was thermally stratified during the study, with a thermocline around 20 m depth. The bottom waters had an average temperature of 15°C (Figure 3a). The pH declined from 7.86 at the lake surface to 6.74 at 73 m depth (Figure 3b). HCO_3^- concentrations ranged from 222 mg L^{-1} at the surface to 260 mg L^{-1} at the lake floor. We modeled the CO_2 concentration dissolved at depth at both sites S1 and S2 using the chemical composition of the lake water (Table 1) and the speciation program PhreeqcI [*Parkhurst and Appelo*, 1999].The calculated CO_2 concentration on the lake floor at S1 and S2 is calculated as

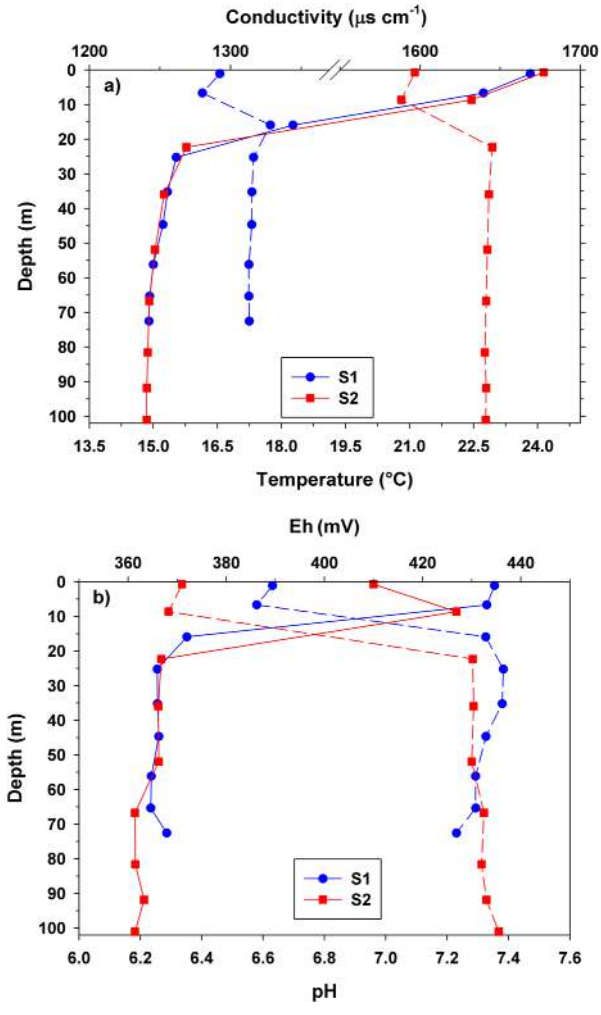

Figure 3. Vertical profiles of (a) the temperature (°C) in solid lines, conductivity in dashed lines (µs cm^{-1}), (b) pH in solid lines and Eh (mV) in dashed lines for S1 and S2.

Table 2. Chemical Composition of Bubbling Gases

	S1	S3
O_2 (vol %)		1.49
N_2 (vol %)		4.58
Ar (vol %)		0.079
CO (vol %)		0.000273
CH_4 (vol %)		0.042
CO_2 (vol %)		93.8
He (vol %)		0.01
R/Ra	7.37	7.03
He/Ne	29.1	9.3
$CO_2/^3He$	8.85×10^8	9.08×10^8
$[He]_{corrected}$ (ppm)	330.6	45.6
$[Ne]_{corrected}$ (ppm)	11.3	4.9
$R/Ra_{corrected}$	7.44	7.24

1.96 mmol kg^{-1}, whereas close to the lake surface it is 0.106 mmol kg^{-1}.

[15] Before reaching the lake surface, a significant proportion (90−95%) of the CO_2 is dissolved in the water due to the pH (from 6.5 to 7.9) which promotes the dissolution, and the transfer of CO_2 from gas bubbles to the water column. As an example, by using the water composition on the lake floor at S1 (Table 1), the program PhreeqcI and the volume of the lake (456,000,000 m^3) an estimation of about 39,284 t of CO_2 is trapped in the lake.

6.2. Dissolved and Bubbling Gases

[16] The bubbling gases sampled at S3 are CO_2 rich and characterized by a relatively high helium concentration (0.01 vol %; Table 2). The chemical composition of both dissolved and bubbling gases have O_2/N_2 ratio about 0.3, lower than the air-saturated water (0.54) highlighting consumption of oxygen. The helium isotope composition of the bubbling gases are 7.44 and 7.24 $R/Ra_{corrected}$, values just below mid-ocean ridge basalt (MORB) values, with He/Ne of 29.1 and 9.3 for S1 and S3, respectively (Table 2). The high $R/Ra_{corrected}$ values indicate a strong contribution of mantle He. He/Ne ratio for S3 is lower than for S1 suggesting air contamination in the S3 sample. $CO_2/^3He$ are 8.85×10^8 and 9.08×10^8 for S1 and S3, respectively, lower than MORB like ratio (1.41×10^9) [*Marty and Jambon*, 1987]. As the gas discharging at 73 m depth was sampled at the surface of S1, the lower value of $CO_2/^3He$ is related to differential dissolution of CO_2 and He in lake water as CO_2 is more soluble than He. Samples collected by *Giggenbach et al*. [1993] showed results of $CO_2/^3He$ ratios around 10–20 $\times 10^9$ on the east side of the Taupo Volcanic Zone and a value of 21 $\times 10^9$ for Tarawera fumarole. The authors attributed this high value to a possible contamination of CO_2 coming from subducted sediments.

[17] The $\delta^{13}C_{TDIC}$ values for the dissolved gases from Lake Rotomahana are 4.23 and 4.72‰ PDB (Table 3) and support the evidence that CO_2 dissolved is not of pure organic origin ($\delta^{13}C = -25‰$) [*Faure*, 1986]. But these values are much higher than the expected isotopic composition for a magmatic source (White Island, $\delta^{13}C \sim -2‰$) [*Giggenbach*, 1995]. For example, Lake Nyos and Lake Monoun (Cameroon) are characterized by $\delta^{13}C_{TDIC}$ values of −3.4‰ to −6.7‰, respectively [*Kusakabe et al*., 1989].

[18] However, the isotope composition of CO_2 gas ($\delta^{13}C_{CO2}$) in equilibrium with the lake was calculated using chemical and isotope mass balance, the temperature of the lake and the concentrations of CO_2 and HCO_3^- in the dissolved gas and water, respectively [*Mook et al*., 1974; *Deines et al*., 1974]. Determination of $\delta^{13}C_{CO2}$ is explained in detailed in *Inguaggiato et al*. [2010]. The obtained values for $\delta^{13}C_{CO2}$ are −2.88 and −2.39‰ (Table 3), suggesting that the difference between $\delta^{13}C_{TDIC}$ and $\delta^{13}C_{CO2}$ can be explained by the fractionation among dissolved C species and free CO_2 [*Mook et al*., 1974; *Inguaggiato et al*., 2000], and therefore the $\delta^{13}C_{CO2}$ values indicate a clear magmatic origin.

6.3. CO_2 Degassing at the Interface Between Lake Surface and the Atmosphere

[19] Results from graphical statistical analysis of the CO_2 flux data are listed in Table 4. The arithmetic mean CO_2 fluxes and 90% confidence intervals (CI) of the mean are estimated using the Sichel t-estimator. A plot of the distribution of CO_2 fluxes shows three populations of data (Figure 4). Population A includes 5% of the lake area (0.5 km^2) with a mean CO_2 flux value of 1831 g m^{-2} d^{-1} (CI = 946–6134 g m^{-2} d^{-1}). Population B includes 93.5% of the lake (9 km^2) with a mean

Table 3. Chemical Composition of Dissolved Gases at S3 Sampled at the Surface (mL L^{-1})[a]

Date	O_2	N_2	CO	CH_4	CO_2
22 Apr 2010	3.88	13.15	1.58×10^{-5}	3.07×10^{-3}	15.84
	3.68	13.65	1.28×10^{-5}	3.71×10^{-3}	19.60

Date	$\delta^{13}C_{TDIC}$	$\delta^{13}C_{CO2}$ computed
27 Apr 2012	4.23	−2.88
	4.72	−2.39

[a]The carbon isotope composition is expressed in ‰ PDB standard.

Table 4. Proportions of Each Population With Their Mean CO_2 Flux (g m^{-2} d^{-1}) and the Flux Range in the 90% Confidence Interval (g m^{-2} d^{-1}) Obtained Using a Statistical Graphical Approach

Population of CO_2 Flux	Proportion of Samples (%)	Mean CO_2 Flux (g m^{-2} d^{-1})	CO_2 Flux Range: 90% Confidence Interval (g m^{-2} d^{-1})
A	5	1297	670–4343
B	94	25	23–28
C	1	0.1	0.06–0.26

CO_2 flux of 25 g m^{-2} d^{-1} (CI = 23–28 g m^{-2} d^{-1}). Population C includes 1.5% of the lake with a mean CO_2 flux of 0.2 g m^{-2} d^{-1} (CI = 0.13–0.66 g m^{-2} d^{-1}). The high mean CO_2 flux value of population A is due to sublacustrine vents discharging CO_2 into the lake, and is confirmed by intense bubble plumes on the surface of the lake as well as by imaging SONAR. The origin of lowest CO_2 fluxes, represented by population C, is not known. Since this population represents only 1.5% of the total, the possible origin could be the absorption of CO_2 via biological activity of algae thereby decreasing the CO_2 diffusion to the atmosphere. This phenomenon has been observed and explained elsewhere [i.e., *Schindler et al*., 1997; *Matthews et al*., 2003].

[20] Population B represents the flux (F_{CO2}) by diffusion at the air-water boundary, and can be explained using a thin boundary layer model [e.g., *Liss and Slater*, 1974]. This model considers a thin film between the water and the atmosphere. The flux by diffusion is calculated by an empirical equation similar to the first Fick's law equation [e.g., *McGillis and Wanninkhof*, 2006]

$$F_{CO2}(\text{g m}^{-2}\ \text{d}^{-1}) = k_{CO2} \times (C_w - C_{w/a}) \times 240 \quad (1)$$

where k_{CO2} is the gas transfer velocity (in cm h^{-1}) for CO_2, C_w and $C_{w/a}$ refer to the concentration of CO_2 in water and in the water film at the water-air interface, respectively. The constant 240 is the conversion factor between units of mg cm^{-2} h^{-1} and g m^{-2} d^{-1}.

[21] Several approaches exist for estimating k_{CO2} [*Frankignoulle et al*., 1996; *Upstill-Goddard et al*., 1990; *McGillis et al*., 2001; *Zappa el al*., 2003; *Clark et al*., 1994]. This coefficient is dependent on the diffusion rate and the wind speed and cannot be measured directly. However, the wind speed can be measured in situ and k_{CO2} is derived from a function of this parameter [*Liss and Merlivat*, 1986; *Wanninkhof*, 1992; *Nightingale et al*., 2000; *Frankignoulle et al*., 1996; *Zhao and Xie*, 2010].

[22] To evaluate the impact of wind speeds on CO_2 flux we revisited 10 high flux sites, which lack bubble plumes, on a windless day and performed a set of replicate flux measurements. The original measurements were performed on 17 December 2010 with a mean wind speed of 4.7 m s^{-1}. We found that the CO_2 flux was on average 75% lower than compared to CO_2 flux when wind speeds were higher. This suggests that the measured CO_2 flux corresponds to CO_2 diffusion at the lake-atmosphere interface and is amplified by the wind. For these sites, the CO_2 flux and maximum wind speed have a good correlation ($R^2 = 0.88$) showing that increased wind speed (which creates larger waves) strongly enhances gas transfer [*Zhao and Xie*, 2010]. These 10 sites were chosen because the area was clear from bubbles at the bottom (echo sounder); the other sites, where CO_2

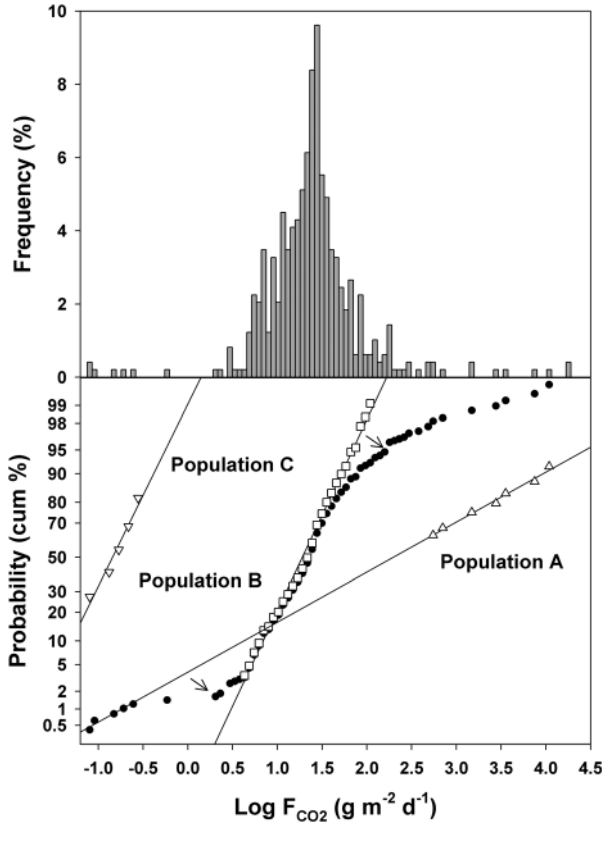

Figure 4. Histogram and probability plot of CO_2 flux data (black circles). Populations A (open triangles up), B (open squares), and C (open triangles down) are shown as straight lines. The inflection point is indicated by an arrow and corresponds to the percentage of each population.

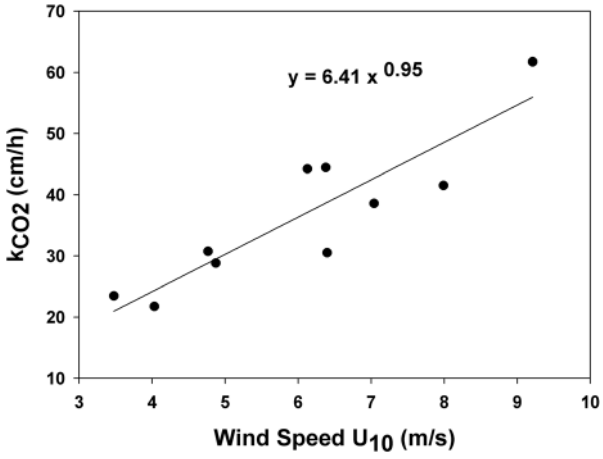

Figure 5. k_{CO2} data plotted against wind speed at 10 m (U_{10}). $U_{10} = u_1 \times 1.29$ (u_1 is the wind speed measured at 1 m height) [*Liss and Merlivat*, 1986].

flux is represented by population B, were rather inconclusive from our observations.

[23] Given this findings, we decided to use these parameters (wind speed and water temperature) to calculate a more appropriate k_{CO2} for Lake Rotomahana. From Figure 5, the derived formula is

$$k_{CO2} = 6.41 \times u_{10}^{0.95} \times [Sc_{CO2}/600]^{-1/2} \quad (2)$$

where u_{10} is the wind speed corrected to a height of 10 m under neutral air boundary conditions ($u_{10} = u_1 \times 1.29$ (u_1 is the wind speed measured at 1 m height)) [*Liss and Merlivat*, 1986], Sc is the Schmidt Number defined as the kinematic viscosity of water at the measured temperature divided by the diffusivity of the gas at that temperature. The transfer velocity k_{CO2} was normalized to a Schmidt number of 600, corresponding to the value for dissolved atmospheric CO_2 in fresh water at 20°C.

[24] The Sc_{CO2} is a function of water temperature as [*Wanninkhof*, 1992]

$$Sc_{CO2} = 1911.1 - 118.11 \times t + 3.4527 \times t^2 - 0.04132 \times t^3 \quad (3)$$

where t is the water temperature (in °C).

[25] The Sc_{CO2} at our measured average daytime surface water temperature of 23.6°C is 504. At an average wind speed u_1 of 2.4 m s^{-1}, k_{CO2} is thus calculated as 20.5 cm h^{-1}.

[26] The value for C_w (equation (1)) was obtained by analyzing dissolved CO_2 concentration and pH in the water sampled at the lake surface and was calculated using the PhreeqcI code. C_w is equal to 0.0047 mg cm^{-3}. The value for $C_{w/a}$ is assumed to be the same as the concentration of CO_2 in the air-saturated water at standard temperature and pressure (STP; 10^{-5} mg cm^{-3}).

[27] From equation (1) with k_{CO2} of 20.5 cm h^{-1} and C_w of 0.0047 (mg cm^{-3}), we estimate the mean CO_2 flux by diffusion to the atmosphere as 23 g m^{-2} d^{-1} which is similar to the value of F_{CO2} (25 g m^{-2} d^{-1}) we measured at the lake surface (i.e., population B).

[28] In summary, only 5% of the degassing of CO_2 at Lake Rotomahana is due to degassing through bubble plumes. The remainder is via diffusion at the surface of the lake. In other words, the majority of CO_2 discharging from lake floor vents dissolves in the water column of the lake and escapes to the atmosphere via diffusion mechanism.

6.4. CO_2 Budget From the Lake

[29] On the basis on the variogram model, 500 sequential Gaussian simulations were performed over a grid of 3851 square cells (50 × 50 m) covering an area of 9.63 km^2 (Figure 6). The average CO_2 output estimated by this method was 549 ± 72 t d^{-1}. CO_2 emission to the atmosphere from the Lake Rotomahana is quite significant if compared with another New Zealand volcanic lake, Ruapehu which has a total CO_2 output of 96 t d^{-1} [*Christenson et al.*, 2010a] and El Chichon volcanic lake located in Mexico (164 t d^{-1}) [*Mazot et al.*, 2011].

[30] The hydrothermal system of Rotomahana is understood to be in steady state since the last eruption in 1886 and consequently, the CO_2 volcanic hydrothermal input to the lake is constant. To quantify the different carbon contributions (CO_2 only) to the total carbon budget of the lake, a simplified mass balance equation can be formulated as follows:

$$C_{input} = C_{storage} - C_{sink} + C_{diffusive\,loss} + C_{bubble\,loss} \quad (4)$$

where the carbon input from the hydrothermal system (C_{input}) can be balanced with the CO_2 emission to the atmosphere through the bubbles ($C_{bubble\ loss}$) and through diffusion ($C_{diffusive\ loss}$), plus storage ($C_{storage}$) and minus sinks (C_{sink}).

[31] $C_{storage}$ (burial rate) in boreal lakes was estimated to be between 0.2 and 0.5 g_{CO2} m^{-2} d^{-1} [*Tranvik et al.*, 2009], our data indicate carbon

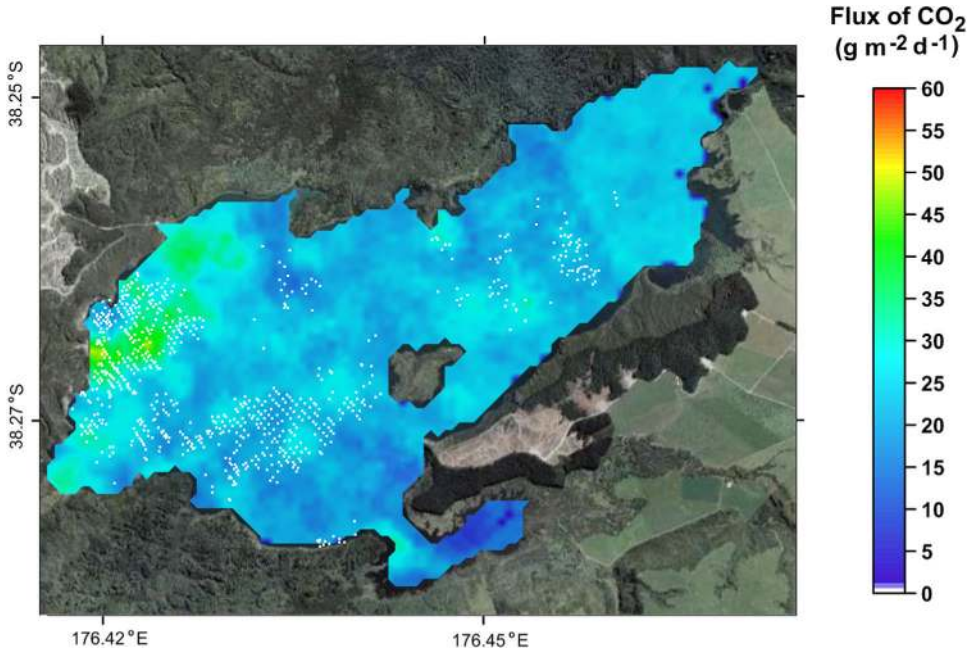

Figure 6. CO_2 flux map (in g m^{-2} d^{-1}) obtained by the 500 sequential Gaussian simulations and probability map of CO_2 flux (see text for explanation). The white points are the bubble plumes seen on the echo sounder.

burial rates for Lake Rotomahana are between 2 and 5 t d^{-1}.

[32] The removal of carbon from the lake as a sink (C_{sink}) would occur from mineral precipitation and biotic uptake. The geochemical Phreeqci modeling [*Parkhurst and Appelo*, 1999] indicates no carbonate precipitation. Biotic uptake of CO_2 from a geochemical study in a boreal lake [*Lopez Bellido et al*., 2009] showed actually that the ecosystem respiration exceeded photosynthesis and so freshwater lakes acted as a source of CO_2 to the atmosphere ($-C_{sink}$). CO_2 flux from the lake to the atmosphere in that study was estimated to be 0.6–0.8 g_{CO2} m^{-2} d^{-1}. So the studies of other lakes suggest that biogenic carbon to the atmosphere is very low.

[33] The main components of the carbon budget therefore are $C_{input} = C_{diffusive\ loss} + C_{bubble\ loss} = 549$ t d^{-1}.

[34] As explained in section 2, the Rotomahana system is part of a bigger hydrothermal system including the Waimangu geothermal system. 44 soil CO_2 flux measurements were performed on the site in 2006 (unpublished data). The average CO_2 flux was 111 g m^{-2} d^{-1} and ranged from 6 to 2765 g m^{-2} d^{-1}. These data support the fact that the mean CO_2 flux from Waimangu is high. The total CO_2 output from the Waimangu/Rotomahana system was estimated to be 1000 t d^{-1} by integrating the Waimangu area (4.4 km^2) to Lake Rotomahana and using the CO_2 output calculated in this study.

6.5. Total CO_2 Emission From the Lake and Tectonic Structures

[35] At least 100 vents (separate bubble plumes) were mapped on the lake floor by the M/V *Taitum* with a Lowrance HDS echo sounder (Figure 6). Carbon dioxide flux maps show that the high CO_2 emission areas are located near the western margin of the lake close to the Steaming Cliffs (Figure 2). High CO_2 fluxes were also measured in the southeastern part of the lake where no hydrothermal activity is present apart from bubbling at the bottom of the lake (Figure 6).

[36] The high CO_2 flux measured at the surface of Lake Rotomahana shows that the geothermal system including Waimangu associated with it is still active and is driven by magmatic degassing. From *Villamor et al*. [2011], the magma appears to be located at depth >10 km. The dike system that created the Tarawera Rift in 1886 could provide pathways for CO_2 to enter the hydrothermal system and so to the lake. In the assumption of a constant CO_2 flux equal to that measured in this work (549 ± 72 t d^{-1}), the total annual emission is 200,385 t of CO_2. Assuming the basaltic magma at depth has a density of 2700 kg m^{-3} and contains around 2 wt % CO_2 (e.g., the value given for Etna

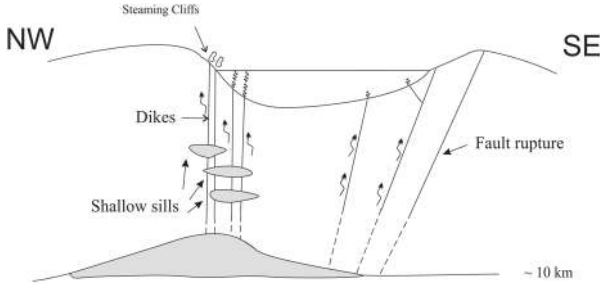

Figure 7. Schematic NW-SE cross section of Rotomahana hydrothermal system. The arrows show possible CO_2 ascent pathways.

by *Aiuppa et al*. [2007]), then 0.0037 km^3 of magma degasses to produce the observed emissions during 1 year. This amount of magma, when integrated over the estimated repose period for Tarawera (~700 years) [*Shane et al*., 2008], is of the same order of magnitude as the 1886 erupted volume (~2 km^3) [*Walker et al*., 1984].

[37] A series of large hydrothermal eruptions occurred across the Waiotapu geothermal field, 10 km south of Lake Rotomahana (Figure 1), at about the same period of time as the ~AD1315 "Kaharoa" rhyolite magmatic eruptions from Tarawera volcano vents, 10–20 km distant. The study of the alteration mineralogy of the hydrothermal eruption deposits and fluid inclusions (CO_2 concentration <0.59 mol kg^{-1}) in drill core samples from Waiotapu geothermal wells (water inflow = 440 kg s^{-1}) [*Hedenquist*, 1991] showed a CO_2 pulse of ~1000 t d^{-1}. From *Nairn et al*. [2005], this pulse was derived from basalt intruded at depth.

[38] Figure 7 shows a model cross section below Lake Rotomahana with the possible pathways for CO_2 to escape to the surface. In the northwest part of the lake close to the Steaming Cliffs area, the 1886 eruption excavated preexisting conduits beneath Lake Rotomahana (sills) and created new fluid pathways to the surface. In the south of the Waimangu/Rotomahana hydrothermal system (Ngakuru fault domain), deep faults with a 60° dip and minor faults forming narrow grabens were found [*Villamor et al*., 2011]. This structure should be present in the southern part of the lake as well, suggesting another pathway for CO_2 to escape to the surface and beneath Lake Rotomahana. It is highly likely that the bubble vents identified at the lake floor are associated not only with the Haroharo caldera rim structure [*Nairn*, 2002] but also with these grabens.

7. Conclusions: CO_2 Emission in the Taupo Volcanic Zone

[39] Comparing the CO_2 flux calculated for Lake Rotomahana with other geothermal systems and volcanoes, we find it to be about half of the CO_2 discharge rate estimated for the nearby Rotorua geothermal system (>1000 t d^{-1}), located close by OVC [*Werner and Cardellini*, 2006] and about 25% of the discharge from White Island volcano (>2000 t d^{-1}), a passively degassing volcano in the Taupo Volcanic Zone [*Werner et al*., 2008].

[40] Studies on Lake Rotomahana have shown the lake is fed by fluids from at least 100 lake floor vents, most of them located in the north-western and south-eastern part of the lake. The total CO_2 output estimated at the surface of the lake is 549 ± 72 t d^{-1}. The main mechanism of CO_2 transfer from the lake to the atmosphere is by diffusion and our study showed that CO_2 flux depends greatly on the wind speed. We developed a new formula for calculated k_{CO2}, and so CO_2 flux by diffusion, specifically for the Lake Rotomahana.

[41] The source of the CO_2 is interpreted to be the magmatic mush zone located at ~10 km depth. The gas rises along pathways caused by the Tarawera eruption in 1886, along the Haroharo caldera rim and along faults that form narrow grabens. The chemical and isotopic composition of dissolved and bubbling gases suggest that (1) there is a strongly contribution of mantle He with $R/Ra_{corrected}$ close to MORB values and (2) the origin of CO_2 is magmatic.

[42] This study showed that the continuous CO_2 emission from Lake Rotomahana is quite significant and the Rotomahana/Waimangu volcanic system is still active, since its 1886 eruption.

Acknowledgments

[43] This manuscript benefited from the thoughtful and constructive reviews of Tony Hurst, Ed Mroczek, Gill Jolly, Deborah Bergfeld, and anonymous reviewers. We thank Heather Bickerton from University of Canterbury for her fieldwork assistance. This research was supported in part by New Zealand Ministry of Business, Innovation and Employment core research funding to GNS Science under the Natural Hazards Research Platform.

References

Aiuppa, A., R. Moretti, C. Federico, G. Giudice, S. Gurrieri, M. Liuzzo, P. Papale, H. Shinohara, and M. Valenza (2007), Forecasting Etna eruptions by real-time observation of

volcanic gas composition, *Geology*, *35*, 1115–1118, doi: 10.1130/G24149A.1.

Bernard, A., and A. Mazot (2004), Geochemical evolution of the young crater lake of Kelud volcano in Indonesia, in *Water-Rock Interaction*, edited by R. B. Wanty and R. R. Seal II, pp. 87–90, A. A. Balkema, New York.

Bernard, A., C. D. Escobar, A. Mazot, and R. E. Guttierrez (2004), The acid crater lake of Santa Ana volcano, El Salvador, *Geol. Soc. Am. Spec. Pap.*, *375*, 121–133.

Capasso, G., and S. Inguaggiato (1998), A simple method for the determination of dissolved gases in natural waters. An application to thermal waters from Vulcano Island, *Appl. Geochem.*, *13*, 631–642.

Cardellini, C., G. Chiodini, and F. Frondini (2003), Application of stochastic simulation to CO_2 flux from soil: Mapping and quantification of gas release, *J. Geophys. Res.*, *108*(B9), 2425, doi:10.1029/2002JB002165.

Chiodini, G., R. Cioni, M. Guidi, B. Raco, and L. Marini (1998), Soil CO_2 flux measurements in volcanic and geothermal areas, *Appl. Geochem.*, *13*, 543–552.

Chiodini, G., F. Frondini, C. Cardellini, D. Granieri, L. Marini, and G. Ventura (2001), CO_2 degassing and energy release at Solfatara volcano, *J. Geophys. Res.*, *106*(B8), 16,213–16,221.

Christenson, B. W., A. Mazot, and K. Britten (2010a), Gas transfer through Ruapehu Crater Lake: Insights gained from a recent water-borne survey, Abstract V23A-2388 presented at 2010 Fall Meeting, AGU, San Francisco, Calif., 13–17 Dec.

Christenson, B. W., A. G. Reyes, R. Young, A. Moebis, S. Sherburn, J. Cole-Baker, and K. Britten (2010b), Cyclic processes and factors leading to phreatic eruption events: Insights from the 25 September 2007 eruption through Ruapehu Crater Lake, New Zealand, *J. Volcanol. Geotherm. Res.*, *191*, 15–32.

Clark, J. F., R. Wanninkhof, P. Schlosser, and H. J. Simpson (1994), Gas-exchange rates in the tidal Hudson River using a dual tracer technique, *Tellus, Ser. B*, *46*, 274–285.

de Ronde, C. E. J., et al. (2002), Discovery of active hydrothermal venting in Lake Taupo, New Zealand, *J. Volcanol. Geotherm. Res.*, *115*, 255–273.

Deines, P., D. Langmuir, and R. S. Harman (1974), Stable carbon isotope ratios and the existence of a gas phase in the evolution of carbonate ground waters, *Geochim. Cosmochim. Acta*, *38*, 1147–1164.

Deutsch, C. V., and A. G. Journel (1998), *GSLIB: Geostatistical Software Library and User's Guide*, Oxford Univ. Press, New York.

Faure, G. (1986), *Inorganic Geochemistry*, Macmillan, New York.

Frankignoulle, M., J.-P. Gattuso, R. Biondo, I. Bourge, G. Copin-Montégut, and M. Pichon (1996), Carbon fluxes in coral reefs. II Eulerian study of inorganic carbon dynamics and measurement of air-sea CO_2 exchanges, *Mar. Ecol. Prog. Ser.*, *145*, 123–132.

Giggenbach, W. F. (1995), Variations in the chemical and isotopic composition of fluids discharged from the Taupo Volcanic Zone, New Zealand, *J. Volcanol. Geotherm. Res.*, *68*, 89–116.

Giggenbach, W. F., Y. Sano, and H. Wakita (1993), Isotopic composition of helium, and CO_2 and CH4 contents in gases produced along the New Zealand part of a convergent plate boundary, *Geochim. Cosmochim. Acta*, *57*, 3427–3455.

Goovaerts, P. (2001), Geostatistical modelling of uncertainty in soil science, *Geoderma*, *103*, 3–26.

Hedenquist, J. W. (1991), Boiling and dilution in the shallow portion of the Waiotapu geothermal system, New Zealand, *Geochim. Cosmochim. Acta*, *55*, 2753–2765.

Inguaggiato, S., G. Pecoraino, and F. D'Amore (2000), Chemical and isotopical characterisation of fluid manifestations of Ischia Island (Italy), *J. Volcanol. Geotherm. Res.*, *99*, 151–178.

Inguaggiato, S., S. Hidalgo, B. Beate, and J. Bourquin (2010), Geochemical and isotopic characterization of volcanic and geothermal fluids discharged from the Ecuadorian volcanic arc, *Geofluids*, *10*, 525–541, doi:10.1111/j.1468-8123.2010.00315.x.

Kusakabe, M., T. Ohsumi, and S. Aramaki (1989), The Lake Nyos gas disaster: Chemical and isotopic evidence in waters and dissolved gases from three Cameroonian crater lakes Nyos, Monoun, and Wum, *J. Volcanol. Geotherm. Res.*, *39*(2–3), 167–185.

Liss, P. S., and L. Merlivat (1986), Air-sea gas exchange rates: Introduction and synthesis, in *The Role of Air-Sea Gas Exchange in Geochemical Cycling*, edited by P. Buat-Menard, pp. 113–127, D. Reidel, Norwell, Mass.

Liss, P. S., and P. G. Slater (1974), Flux of gases across the air-sea interface, *Nature*, *247*, 181–184.

Lopez Bellido, J., T. Tulonen, P. Kankaala, and A. Ojala (2009), CO_2 and CH_4 fluxes during spring and autumn mixing periods in a boreal lake (Paajarvi, southern Finland), *J. Geophys. Res.*, *114*, G04007, doi:10.1029/2009JG000923.

Marty, B., and A. Jambon (1987), $C/^3He$ in volatile fluxes from the solid Earth: Implications for carbon geodynamics, *Earth Planet. Sci. Lett.*, *83*, 16–26.

Matthews, C. J. D., V. L. St Louis, and R. H. Hesslein (2003), Comparison of three techniques used to measure diffusive gas exchange from sheltered aquatic surfaces, *Environ. Sci. Technol.*, *37*, 772–780.

Mazot, A., D. Rouwet, Y. Taran, S. Inguaggiato, and N. Varley (2011), CO_2 and He degassing at El Chichon volcano, Chiapas, Mexico: Gas flux, origin and relationship with local and regional tectonics, *Bull. Volcanol.*, *73*, 423–441, doi:10.1007/s00445-010-0443-y.

McGillis, W. R., and R. Wanninkhof (2006), Aqueous CO_2 gradients for air-sea flux estimates, *Mar. Chem.*, *98*, 100–108, doi:10.1016/j.marchem.2005.09.003.

McGillis, W. R., J. B. Edson, J. D. Ware, J. W. H. Dacey, J. E. Hare, C. W. Fairall, and R. Wanninkhof (2001), Carbon dioxide flux techniques performed during GasEx 98, *Mar. Chem.*, *75*, 267–280.

Mongillo, M. (1994), Aerial thermal infrared mapping of the Waimangu-Waiotapu geothermal region, New Zealand, *Geothermics*, *23*, 511–526.

Mook, W. G., J. C. Bommerson, and W. H. Staverman (1974), Carbon isotope fractionation between dissolved bicarbonate and gaseous carbon dioxide, *Earth Planet. Sci. Lett.*, *22*, 169–176.

Nairn, I. A. (2002), Geology of the Okataina Volcanic Centre, Geological Map 25, 156 p, Inst. of Geol. and Nucl. Sci., Lower Hutt, New Zealand.

Nairn, I. A., J. W. Hedenquist, P. Villamor, K. R. Berryman, and P. A. Shane (2005), The ~AD1315 Tarawera and Waiotapu eruptions, New Zealand: Contemporaneous rhyolite and hydrothermal eruptions driven by an arrested basalt dike system?, *Bull. Volcanol.*, *67*, 186–193, doi:10.1007/s00445-004-0373-7.

Nightingale, P. D., G. Malin, C. S. Law, A. J. Watson, P. S. Liss, M. I. Liddicoat, J. Boutin, and R. C. Upstill-Goddard (2000), In situ evaluation of air-sea gas exchange

parameterizations using novel conservative and volatile tracers, *Global Biogeochem. Cycles*, *14*(1), 373–387.

Parkhurst, D. L., and C. A. J. Appelo (1999), User's guide to PHREEQC—A computer program for speciation, batch-reaction, one-dimensional transport, and inverse geochemical calculations, *U.S. Geol. Surv. Water Resour. Invest. Rep.* 99–4259, 312 pp., Denver, Colorado, USA.

Perez, N. M., et al. (2011), Global CO_2 emission from volcanic lakes, *Geology*, *39*, 235–238, doi:10.1130/G31586.1.

Sano, Y., H. Wakita, T. Ohsumi, and M. Kusakabe (1987), Helium isotope evidence for magmatic gases in Lake Nyos, Cameroon, *Geophys. Res. Lett.*, *14*(10), 1039–1041.

Schindler, D. E., S. R. Carpenter, J. J. Cole, J. F. Kitchell, and M. L. Pace (1997), Influence of food web structure on carbon exchange between lakes and the atmosphere, *Science*, *277*, 248–251.

Shane, P., V. C. Smith, and I. Nairn (2008), Millennial timescale resolution of rhyolite magma recharge at Tarawera volcano: Insights from quartz chemistry and melt inclusions, *Contrib. Mineral. Petrol.*, *156*, 397–411.

Sinclair, A. J. (1974), Selection of threshold values in geochemical data using probability graphs, *J. Geochem. Explor.*, *3*, 129–149.

Tranvik, L. J., et al. (2009), Lakes and reservoirs as regulators of carbon cycling and climate, *Limnol. Oceanogr. Methods*, *54*, 2298–2314.

Upstill-Goddard, R. C., A. J. Watson, P. S. Liss, and M. I. Liddicoat (1990), Gas transfer in lakes measured with SF6, *Tellus, Ser. B*, *42*, 364–377.

Varekamp, J. C., G. B. Pasternack, and G. L. Rowe (2000), Volcanic lake systematics II. Chemical constraints, *J. Volcanol. Geotherm. Res.*, *97*, 161–179.

Villamor, P., K. R. Berryman, I. A. Nairn, K. Wilson, N. Litchfield, and W. Ries (2011), Associations between volcanic eruptions from Okataina volcanic center and surface rupture of nearby active faults, Taupo rift, New Zealand: Insights into the nature of volcano-tectonic interactions, *Bull. Volcanol.*, *123*, 1383–1405, doi:10.1130/B30184.1.

Walker, G. P. L., S. Self, and L. Wilson (1984), Tarawera, 1886, New Zealand—A basaltic Plinian fissure eruption, *J. Volcanol. Geotherm. Res.*, *21*, 61–78.

Wanninkhof, R. (1992), Relationship between wind speed and gas exchange over the ocean, *J. Geophys. Res.*, *97*(C5), 7373–7382.

Werner, C., and C. Cardellini (2006), Comparison of carbon dioxide emissions with fluid upflow, chemistry, and geologic structures at the Rotorua geothermal system, New Zealand, *Geothermics*, *35*, 221–238.

Werner, C., T. Hurst, B. Scott, S. Sherburn, B. W. Christenson, K. Britten, J. Cole-Baker, and B. Mullan (2008), Variability of passive gas emissions, seismicity, and deformation during crater lake growth at White Island Volcano, New Zealand, 2002–2006, *J. Geophys. Res.*, *113*, B01204, doi:10.1029/2007JB005094.

Zappa, C. J., P. A. Raymond, E. A. Terray, and W. R. McGillis (2003), Variation in surface turbulence and the gas transfer velocity over a tidal cycle in a macro-tidal estuary, *Estuaries*, *26*, 1401–1415.

Zhao, D., and L. Xie (2010), A practical bi-parameter formula of gas transfer velocity depending on wave states, *J. Oceanogr.*, *66*, 663–671.